



1 SPATIALLY VARYING RELEVANCE OF 2 HYDROMETEOROLOGICAL HAZARDS FOR 3 VEGETATION PRODUCTIVITY EXTREMES

4 Josephin Kroll^{1*}, Jasper M. C. Denissen^{1*}, Mirco Migliavacca¹, Wantong Li¹, Anke Hildebrandt^{2,3,4}, Rene
 5 Orth¹

6
 7 * Authors contributed equally

8
 9 1 – Department of Biogeochemical Integration, Max Planck Institute for Biogeochemistry, Jena,
 10 Germany

11 2 – German Centre for Integrative Biodiversity Research, Halle-Jena-Leipzig, Leipzig, Germany

12 3 - Helmholtz Centre for Environmental Research–UFZ, Leipzig, Germany

13 4 - Friedrich-Schiller-University Jena, Jena, Germany

14
 15 Correspondence: Josephin Kroll (jkroll@bgc-jena.mpg.de) and Jasper M. C. Denissen ([idenis@bgc-](mailto:idenis@bgc-jena.mpg.de)
 16 [jenam.mpg.de](mailto:idenis@bgc-jena.mpg.de))

17 ABSTRACT

18 Vegetation plays a vital role in the Earth system by sequestering carbon, producing food and oxygen,
 19 and providing evaporative cooling. Vegetation productivity extremes have multi-faceted implications,
 20 for example on crop yields or the atmospheric CO₂ concentration. Here, we focus on productivity
 21 extremes as possible impacts of coinciding, potentially extreme hydrometeorological anomalies. Using
 22 monthly global satellite-based Sun-induced chlorophyll fluorescence data as a proxy for vegetation
 23 productivity from 2007 - 2015, we show that vegetation productivity extremes are related to
 24 hydrometeorological hazards as characterized through ERA5-Land reanalysis data in approximately 50%
 25 of our global study area. For the latter, we are considering sufficiently vegetated and cloud-free regions;
 26 and we refer to hydrometeorological hazards as water or energy related extremes inducing productivity
 27 extremes. The relevance of the different hazard types varies in space; temperature-related hazards
 28 dominate at higher latitudes with cold spells contributing to productivity minima and heat waves
 29 supporting productivity maxima, while water-related hazards are relevant in the (sub)tropics with
 30 droughts being associated with productivity minima and wet spells with the maxima. Next to single
 31 hazards also compound events such as joint droughts and heat waves or joint wet and cold spells play
 32 a role, particularly in dry and hot regions. Further, we detect regions where energy control transitions
 33 to water control between maxima and minima of vegetation productivity. Therefore, these areas
 34 represent hot spots of land-atmosphere coupling where vegetation efficiently translates soil moisture
 35 dynamics into surface fluxes such that the land affects near-surface weather. Overall, our results
 36 contribute to pinpoint how potential future changes in temperature and precipitation could propagate
 37 to shifting vegetation productivity extremes and related ecosystem services.

39 1 INTRODUCTION

40 Vegetation is a crucial component of the Earth system because it provides ecosystem services like food
 41 and oxygen production, CO₂ sequestration and evaporative cooling. Therefore, the effects of changes
 42 in vegetation productivity are diverse; it influences crop yields (Orth et al., 2020), cloud formation (Hong



et al., 1995; Freedman et al., 2001), precipitation (Pielke Sr et al., 2007), atmospheric pollution (Otu-Larbi et al., 2019) and heat wave intensity (Li et al., 2021b).
 Photosynthesis requires sufficient water (soil moisture) and energy (incoming shortwave radiation) supply. In regions that are water (energy) limited, plants usually benefit from water (energy) surpluses and suffer from respective deficits. Many studies confirm that, depending on the evaporative regime, vegetation productivity follows the temporal evolution of influential variables such as soil moisture or temperature which summarize the water or energy dynamics (Beer et al., 2010; Seddon et al., 2016; Madani et al., 2017; Denissen et al., 2020; Piao et al., 2020; Li et al., 2021a).
 Correspondingly, hydrometeorological hazards, such as temperature and precipitation extremes have implications on vegetation productivity. Many studies investigated the influence of such hazards on vegetation productivity, highlighting their impact on the biosphere (Ciais et al., 2005; Zhao et al., 2010; Zscheischler et al., 2013; Zscheischler et al., 2014a; Zscheischler et al., 2014b; Flach et al., 2018; Wang et al., 2019; Zhang et al., 2019; Qui et al., 2020). However, usually these studies focus on particular types of hydrometeorological hazards such as droughts or heat waves, or they use vegetation productivity data from models or other proxies rather than the recent satellite-derived Sun-induced chlorophyll fluorescence (SIF) data (Frankenberg et al., 2011; Joiner et al., 2013).
 In this study, we re-visit the relationship between vegetation productivity and hydrometeorological hazards by, to our knowledge, for the first time comprehensively analyzing the implications of both single and compound hazards on observation-based vegetation productivity extremes as inferred from SIF data across the globe. This analysis is done from an impact perspective; we first detect impacts (productivity extremes) before relating them to coinciding, potentially extreme hydrometeorological anomalies (Smith, 2011). Finally, we investigate where the full vegetation productivity range between minima and maxima involves transitions from energy to water controls. In regions where this occurs, the feedback of the land surface on the climate can be stronger, as the water-controlled vegetation translates soil moisture dynamics through its energy and water fluxes to affect the boundary layer and consequently also near-surface weather. Hence, our vegetation-based analysis can indicate hot spots of land-atmosphere coupling (Koster et al., 2004; Guo and Dirmeyer, 2013).
 In section 3.1 we investigate the co-occurrence of vegetation productivity extremes and hydrometeorological hazards. Further, we show the timing of such vegetation productivity extremes in section 3.2. Additionally, we determine the main drivers of vegetation productivity extremes and assess the influence of underlying evaporative regimes in section 3.3. We summarize our results across climate regimes in section 3.4 and investigate regions with vegetation productivity controls switching between water and energy variables in section 3.5.

2 DATA AND METHODS

In order to characterize vegetation behavior, we use SIF and Normalized Difference Vegetation Index (NDVI) data in this study. SIF is used as a proxy for vegetation productivity. We employ satellite-observed SIF data retrieved from the Global Ozone Measurement Experiment (GOME-2; Koehler et al., 2015). In the derivation of this SIF product, multiple corrections for varying solar zenith angles, differences in overpass times and cloud fraction have been applied to yield reliable SIF estimates. In addition to vegetation productivity, we also study changes related to vegetation greenness by using satellite-observed Normalized Difference Vegetation Index (NDVI) data from Moderate-resolution Imaging Spectroradiometer (MODIS; Didan, 2015).
 As for the hydrometeorological variables, representing energy and water availability, we consider 2m temperature, shortwave incoming radiation, vapor pressure deficit, soil moisture from 4 layers (1: 0-7 cm, 2: 7-28 cm, 3: 28-100 cm, 4: 100-289 cm) and total precipitation, all from the ERA5-Land reanalysis data (Muñoz-Sabater, 2019). In addition to this, and to validate the robustness of our results, we use an alternative soil moisture product, SoMo.ml, which provides data for three layers (1: 0-10 cm, 2: 10-30cm, 3: 30-50cm), and which is derived through a machine learning approach that is trained with in-situ soil moisture measurements from across the globe (O and Orth, 2021). All datasets used in this study are summarized in Table 1.



Table 1. Data sets used in this study.

Variables	Dataset	Version	Application	Reference
Sun-induced chlorophyll fluorescence	GOME-2	GFZ	Vegetation productivity proxy	Köhler et al., 2015
Normalized difference vegetation Index	MOD13C1	V006	Vegetation greenness proxy	Didan, 2015
Soil moisture layer 1-4, precipitation, shortwave incoming radiation, temperature, vapor pressure deficit	ERA5 land		Hydrometeorological variables indicating energy and water availability	Muñoz-Sabater, 2019
Precipitation, net solar radiation, net thermal radiation	ERA5		Computation of aridity to evaluate resulting patterns	Hersbach et al., 2020
Soil moisture layer 1-3	SoMo.ml	1	Alternative soil moisture data set	O and Orth, 2021
Fraction of vegetation cover	VCF5KYR	1	Evaluation of resulting patterns with respect to vegetation characteristics	Hansen and Song, 2018

The workflow applied to these datasets is illustrated in Fig. 1. At first, all data is pre-processed for comparability by (i) aggregating it to monthly, half-degree spatial and temporal resolution and by (ii) focusing on the time period 2007–2015. Next, we compute anomalies by removing linear trends and the mean seasonal cycle from the data for both the vegetation and hydrometeorological variables. In each grid cell, we disregard months with an absolute SIF value below $0.5 \text{ mW/m}^2/\text{sr/nm}$ to focus on times with sufficiently active vegetation (as in Li et al., 2021a). Additionally, grid cells with a fractional vegetation cover $< 5\%$ are excluded from the analysis. Finally, we assure the necessary data availability by considering only grid cells with > 15 monthly anomalies across the study period remaining after the filtering. Out of the identified suitable months in each grid cell, we determine the five strongest negative and five strongest positive monthly SIF anomalies. The sum of all grid cells for which five SIF maxima and minima can be detected is referred to as total study area.

After this filtering, we follow two approaches in our analysis. In the first approach, we check for hydrometeorological hazards coinciding with the determined extreme vegetation productivity events. Thereby, we consider air temperature and soil moisture layer 2 as these variables were previously found to be globally most relevant for vegetation productivity (Li et al., 2021a). At first we average the monthly temperature and soil moisture anomalies across the five months of maximum and minimum SIF anomalies. Then, a series of steps is taken to test if the coinciding hydrometeorological anomalies during SIF extremes are actually hazardous: (i) We randomly sample five months with sufficiently active vegetation and average the soil moisture and temperature anomalies, respectively, across them. (ii) We repeat this 100 times to obtain a distribution from which we determine the 10th and 90th percentile. (iii) A hydrometeorological hazard is detected if the actual, averaged temperature and/or soil moisture anomalies associated with the SIF extremes are below 10th (cold spell or drought) or above the 90th percentile (heat wave or wet spell) of the distribution of randomly sampled averaged anomalies. Note that with this approach we can detect both single and compound hydrometeorological hazards.

Complementing this analysis, in the second approach we analyze the temporal co-variation between SIF extremes and hydrometeorological anomalies. For this purpose, we correlate the five SIF extreme anomalies with anomalies of all considered hydrometeorological variables in each grid cell. We include



respective SIF and hydrometeorological data from the surrounding grid cells to yield a larger data sample consisting of $5 \times (8+1) = 45$ data pairs. We disregard negative and insignificant ($p\text{-value} > 0.05$) correlations, as we assume these are not indicating actual physical controls but rather represent the influence of noise or confounding effects such as low precipitation during times of high radiation. Finally, the hydrometeorological variable that yields the highest correlation coefficient with the extreme SIF anomalies is regarded as the main SIF-controlling variable during vegetation productivity maxima or minima.

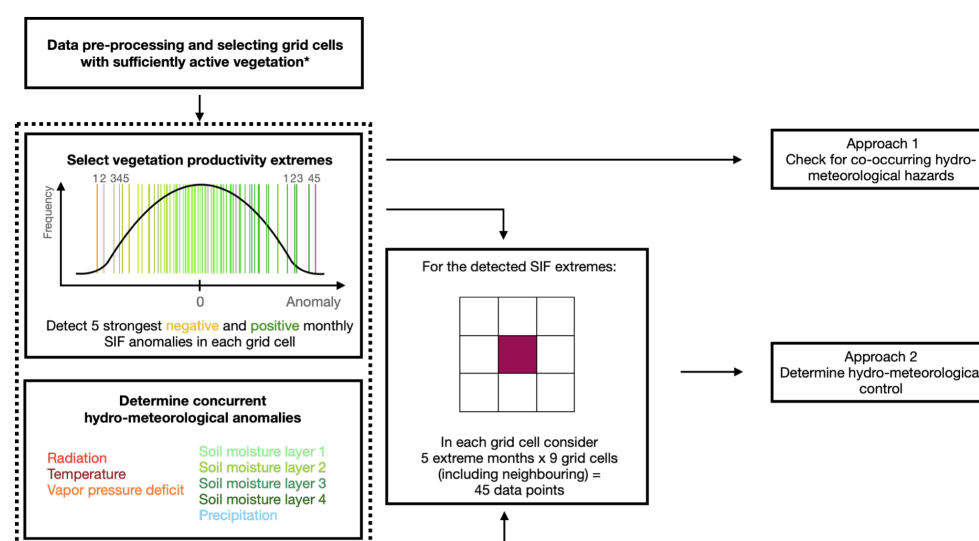


Figure 1. Schematic representation of our methodological approach. *Filtering for sufficiently active vegetation is explained in section 2.

3 RESULTS AND DISCUSSION

3.1 HYDROMETEOROLOGICAL HAZARDS AND VEGETATION PRODUCTIVITY EXTREMES

Figure 2 shows which hydrometeorological hazards are associated with SIF extremes as inferred with approach 1 described in Section 2 and in Fig. 1. In approximately 50% of the global study area, we find that vegetation productivity extremes are associated with hydrometeorological hazards. This is in line with previous research (Zscheischler et al., 2014b). For both maximum and minimum vegetation productivity, we find spatially coherent patterns of associated hydrometeorological hazards. In the Northern Hemisphere SIF maxima (minima) at high latitudes relate to heat waves (cold spells), where in mid latitudes they occur jointly with wet spells (droughts). This suggests that hydrometeorological hazards associated with SIF extremes vary systematically according to energy- and water control of the local vegetation. Thereby, the boundary between both regimes and the respectively determined relevant hydrometeorological hazards is surprisingly sharp, for example in North America, and in eastern Europe and Russia (Flach et al., 2018).

Further, single hydrometeorological hazards (either an extreme temperature or soil moisture anomaly) are relevant in more areas than compound hazards (combination of extreme temperature and extreme soil moisture anomaly). Compound hazards seem to be particularly important in the sub-tropics on both hemispheres. Differences also exist between maximum and minimum vegetation productivity extremes, the latter being slightly more associated with compound hazards.

Overall, the most frequent hazards during vegetation productivity minima are droughts and cold spells. Previous studies have reported the relevance of drought in this context (Zscheischler et al., 2013; Zscheischler et al., 2014a; Zscheischler et al., 2014b) even though for different vegetation productivity



proxies. On the contrary, the importance of cold spells is not analyzed, probably because vegetation productivity in boreal regions is comparably smaller than in e. g. tropical regions (Li and Xiao, 2019). The results in Fig. 2 are based on averages of the five months with strongest SIF anomalies in each grid cell. Figure S1 shows co-occurring hydrometeorological hazards separately for each of the five SIF maxima and minima. The patterns are similar as in Fig. 2, we consistently find temperature-related hazards to be relevant in energy-controlled regions and water-related hazards in water-controlled regions across all five individual SIF extremes. Weaker SIF extremes tend to be less associated with hydrometeorological hazards. This could be because the signal-to-noise ratio is decreased for weaker extremes, or other factors such as disturbances (fire or insect outbreaks) play a more prominent role for these productivity extremes. As mentioned, soil moisture layer 2 is used here to detect droughts and wet spells, but similar results are obtained with soil moisture layers 1 and 3, respectively (not shown).

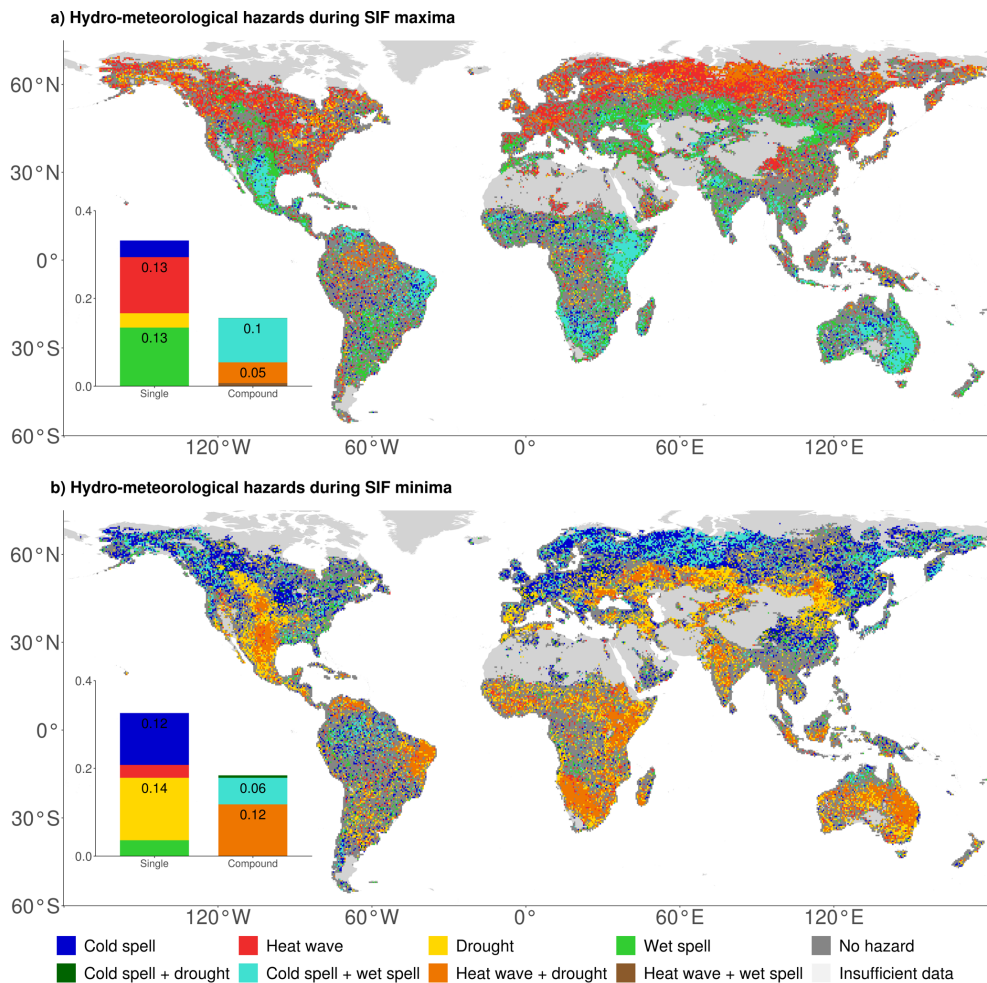


Figure 2. Hydrometeorological hazards co-occurring with (a) SIF maxima and (b) SIF minima. Colors denote the type of hydrometeorological hazard. Bar plots indicate the area affected by each hazard type relative to the total study area.

3.2 TIMING OF STRONGEST SIF EXTREME



To further understand the spatially varying relevance of hydrometeorological hazards, we show the months of the year associated with the strongest SIF extreme in each grid cell in Fig. 3. The spatial pattern is quite different from that in Fig. 2, for example the sharp transitions between regions with energy and water-related hydrometeorological hazards are not present in Fig. 3. Hence, this transition is apparently not related to SIF extremes occurring in different seasons and might be rather related to different evaporative regimes which will be further investigated in the next subsection 3.3. The spatial variability in Fig. 3 is lower at high latitudes compared with (sub-)tropical regions. At high latitudes the growing season is short and constrained by energy availability. In the tropics, we find an increased smaller-scale variability, presumably due to the weak seasonal cycle of hydrometeorological variables. Most SIF extremes in North America and Eurasia occur in the early growing season, presumably when vegetation either starts to grow or growing is limited due to energy or water control. While here we show the months-of-year associated with the strongest SIF extreme, in Fig. S2 we show similar patterns in the timing of the 2nd to 5th strongest SIF extremes, indicating that each of the remaining SIF extremes occurs in similar months-of-year.

a) Maximum

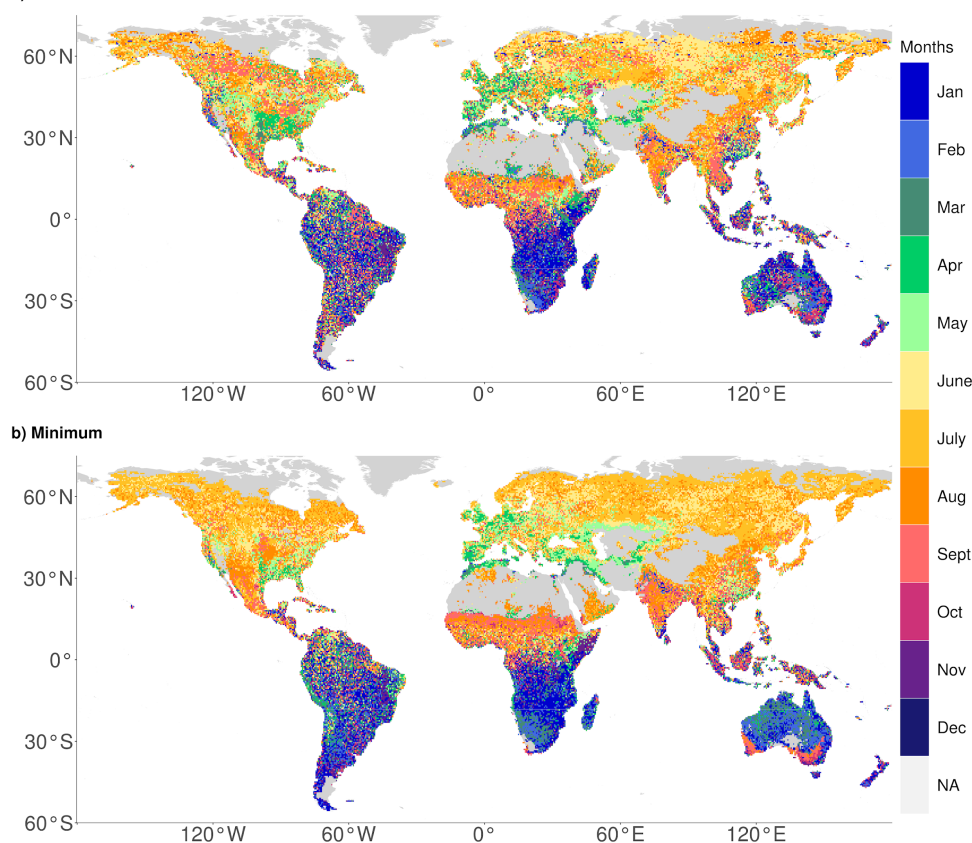


Figure 3. Global distribution of the month-of-year in which the strongest SIF (a) maximum and (b) minimum anomaly occur. Data gaps (grey) are caused by filtering for active vegetation and excluding insignificant and negative correlations.

3.3 HYDROMETEOROLOGICAL DRIVERS OF VEGETATION PRODUCTIVITY EXTREMES

After showing the co-occurrence of hydrometeorological hazards with SIF extremes, we apply a correlation analysis (approach 2 in section 2) to characterize the co-variability between extreme SIF anomalies and concurrent hydrometeorological anomalies. Figure 4 shows the hydrometeorological



196 variable that correlates strongest with SIF during extreme vegetation productivity months, indicating
 197 respective controls. At the high latitudes and in the tropics SIF extremes are generally energy controlled,
 198 while in the mid latitudes and subtropics they are water controlled. Overall, we find similar spatial
 199 patterns as in Fig. 2, demonstrating consistent results across co-occurrence and co-variability of SIF
 200 extremes and hydrometeorological hazards. This coherence suggests that hydrometeorological hazards
 201 play a key role in inducing SIF extremes.
 202 The bar plot insets in Fig. 3 indicate that SIF maxima are predominantly controlled by energy variables
 203 while SIF minima are overall more controlled by water variables. Even though weaker, this shift is also
 204 present in Fig. 2. This difference can be explained with transitional regions, which have energy-
 205 controlled SIF maxima, but water-controlled SIF minima. This is illustrated for example by the northward
 206 shift of the transition between energy and water control in Russia when comparing the results for
 207 maximum and minimum SIF. These transitional regions will be further investigated in section 3.5.
 208 We repeated this analysis with SoMo.ml soil moisture and found similar spatial patterns of energy- and
 209 water-controlled regions (Fig. S3), underlining that our results are robust with respect to the choice of
 210 the soil moisture product. Furthermore, we repeat our co-variability analysis for NDVI instead of SIF in
 211 Fig. S4, which allows us to contrast to some extent the behavior of vegetation physiology (SIF) and
 212 vegetation structure (NDVI). Similar to the spatial patterns of energy- and water-controlled vegetation
 213 in Fig. 4, NDVI shows predominant energy control at high latitudes, while the mid latitudes are largely
 214 water-controlled. Further, as in Fig. 4 for SIF, NDVI minima are more associated with water variables
 215 than NDVI maxima.
 216 However, the overall extent of water-controlled areas is clearly larger in the case of NDVI compared
 217 with the SIF results. This could (i) partly be related to the fact that NDVI, being less dynamic than SIF
 218 because it is more related to vegetation greenness and structure, tends to vary at time scales more in
 219 line with that of soil moisture (Turner et al., 2020), which can support stronger correlations. (ii) It could
 220 be due to confounding effects of the changing soil/vegetation color between dry and wet states on the
 221 NDVI signal. (iii) NDVI tends to saturate for canopies with high Leaf Area Index and tend to be relatively
 222 stable over evergreen boreal forests (Turner et al., 1999; Walther et al., 2015). This can mask significant
 223 correlations between NDVI and energy related variables in the boreal regions that are more energy
 224 controlled (Fig. 4).

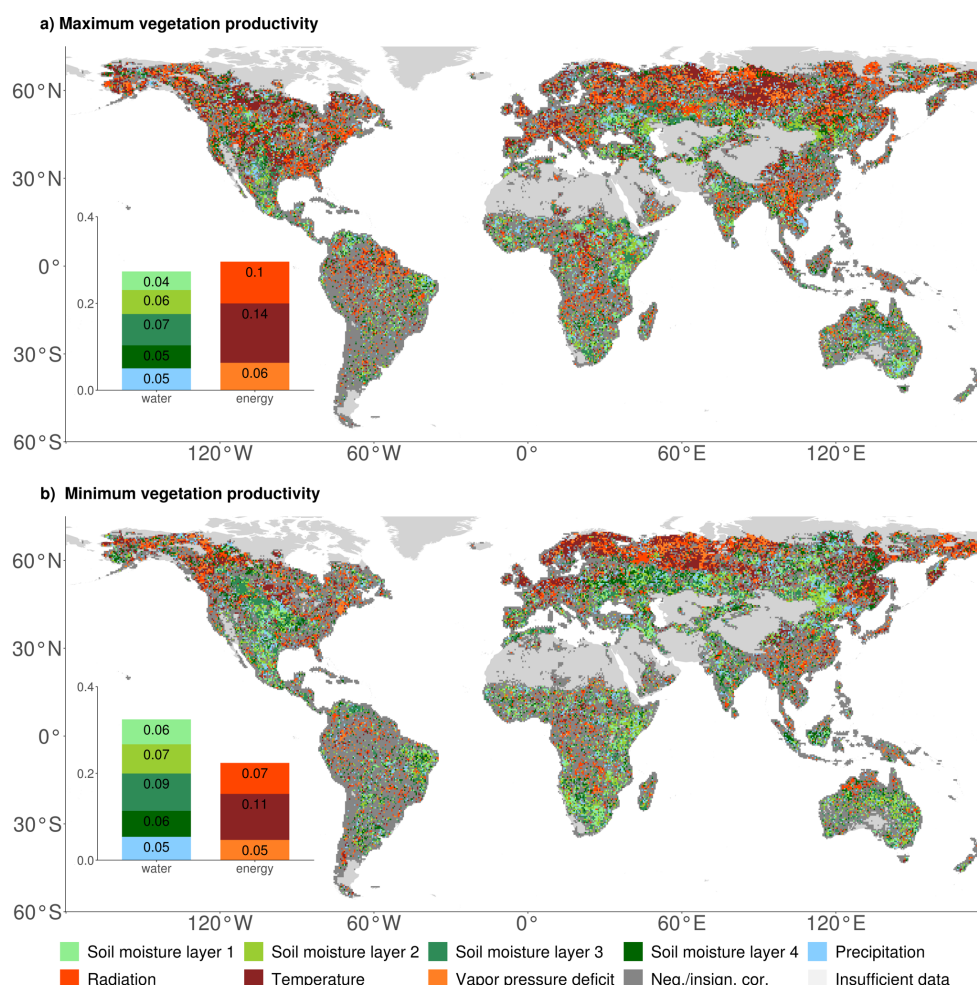


Figure 4. Global distribution of hydrometeorological controls of Sun-Induced Fluorescence (SIF) (a) maxima and (b) minima in respective colors, as assessed from strongest correlations. The inset bar plot indicates the area controlled by each variable relative to the total study area. Dark grey color denotes the study area, in which correlations are negative/insignificant.

3.4 HYDROMETEOROLOGICAL CONTROLS ACROSS CLIMATE REGIMES

In addition to analyzing the spatial variation of the main drivers of vegetation productivity extremes, we attempt to further understand the large-scale patterns along temperature and aridity gradients. To this end, we bin grid cells by their climate characteristics as denoted by long-term mean temperature and aridity (the ratio between unit-adjusted net radiation and precipitation). The results in Fig. 5 illustrate which hydrometeorological variable most often has the highest correlation with SIF anomalies in each climate regime.

Figure 5 (a) and (b) show that vegetation productivity extremes in humid regions (aridity < 1; Budyko, 1974) are mostly energy controlled, with temperature controlling in cold regions (long-term average temperature < 10 °C) and radiation controlling in warm regions (long-term temperature > 10 °C). In contrast, productivity extremes in arid regions (aridity > 2, Budyko, 1974) are mainly water controlled, with soil moisture layer 2 and 3 as most important water controls. The main difference between maximum and minimum SIF results is detectable in semi-arid regions (1 < aridity < 2). While for maximum SIF those climate regimes show mostly energy control, SIF minima in these regimes are largely water controlled. From this, we deduce that semi-arid regions represent the transitional regime, as the



244 main drivers change from energy to water variables from SIF maximum to SIF minimum.
245 The results for NDVI show similar patterns despite an increased overall water control as seen earlier in
246 the global maps (Fig. S4). For example, where in humid regions SIF extremes are mainly energy
247 controlled, NDVI extremes are more often water controlled, which is also reflected in the global maps
248 in Fig. S4.
249 Figure 5 (e) and (f) show the results of Fig. 2 binned according to their long-term climate characteristics.
250 In humid regions, both SIF extremes are co-occurring with temperature hazards. In contrast, in arid
251 regions water-related hazards co-occur with maximum and minimum SIF. Thereby, Fig. 5 underlines
252 once more the similarity of the results obtained with approaches 1 (Fig. 2) and 2 (Fig. 4).
253 To additionally explore the influence of different vegetation types on the main controls of vegetation
254 productivity, we bin the grid cell results by the respective fraction of tree cover of the entire vegetation
255 cover, and by aridity in Fig. S5. We find that the radiation control of SIF extremes in humid regions is
256 mostly associated with forests, and that the water control in semi-arid regions largely occurs for shorter
257 vegetation while productivity extremes in more forested semi-arid regions tend to be energy-controlled.
258 As in Fig. 5, similar patterns are found for NDVI extremes with overall increased relevance of water
259 variables particularly in short vegetation-dominated regions.

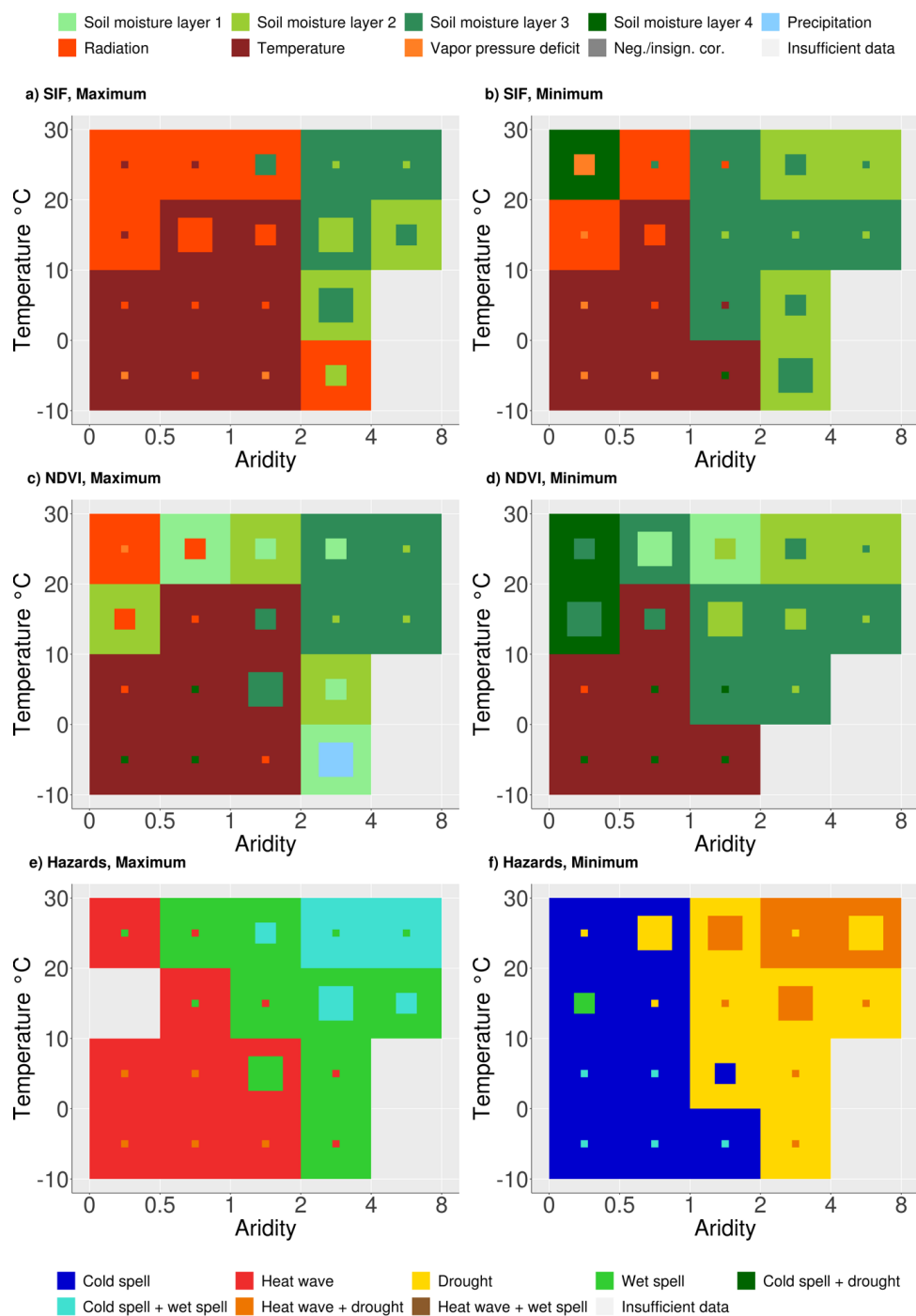


Figure 5. Hydrometeorological controls of vegetation productivity extremes summarized across climate regimes, (a) and (b) for Sun-Induced Fluorescence (SIF) extremes, (c) and (d) for Normalized Difference Vegetation Index (NDVI) extremes. (e) and (f) display the hydrometeorological hazards co-occurring with the SIF extremes. Box color denotes the main controlling



264 hydrometeorological variable, the second most important variable is indicated in the smaller squares' color, while its size
 265 represents the ratio between highest/second highest amounts of grid cells.

266 3.5 SWITCHING HYDROMETEOROLOGICAL CONTROLS BETWEEN SIF MAXIMA AND MINIMA

267 In a final step, we focus on shifts between energy and water control when moving from SIF maxima to
 268 SIF minima. The respective transitional regions represent hot spots of land-atmosphere coupling as (i)
 269 in these regions the land surface (soil moisture) is affecting near-surface weather at least during
 270 productivity minima (therefore also influencing transpiration) and (ii) this effect can be significant as
 271 transpiration (variability) is relatively high compared with drier regions where vegetation productivity
 272 would be water-limited across its entire range from minimum to maximum. The results are depicted in
 273 Fig. 6, which illustrates these emerging transitions from water to energy control (yellow) and vice-versa
 274 (blue, denoting land-atmosphere hot spots). Grid cells that stay within water or energy control, even
 275 with a change between the water or energy variables, respectively, are shown in black indicating no
 276 transition. Figure 6 (a) reveals many regions with no transition. Transitions are found mostly in North
 277 Eurasia and North America. Globally, a change from energy control during maximum SIF to water control
 278 during minimum SIF occurs more often (8% of the study area) than the opposite transition (5%).
 279 Figure 6b and c display the percentage of grid cells in each climate regime changing from water to
 280 energy control and vice-versa with grid cells binned with respect to long-term climate conditions, similar
 281 to Fig. 5. The highest fraction of grid cells in each climate regime would show no change, but as we focus
 282 on transitioning grid cells, only they are displayed. Transitions from water to energy control between
 283 SIF maxima and SIF minima happen most often in cold, humid regions. This is deviating from the
 284 prevailing energy control in these climate regimes, and probably related to local-scale features and/or
 285 micro-meteorological conditions. Figure 6 (c) indicates that changes from energy control during
 286 maximum SIF to water control during minimum SIF most frequently occur in the semi-arid transitional
 287 regions. These are land-atmosphere coupling hot spots as described above. The transition from energy
 288 to water limitation could be caused by energy-controlled maxima in spring, when presumably soil water
 289 resources are available after being replenished during autumn and winter. With sufficient water supply,
 290 energy surpluses could induce vegetation productivity maxima. During summer, soil moisture could be
 291 depleted for example by the high vegetation demand, and therefore taking over the SIF control of
 292 photosynthesis that is reflected into the SIF dynamics.

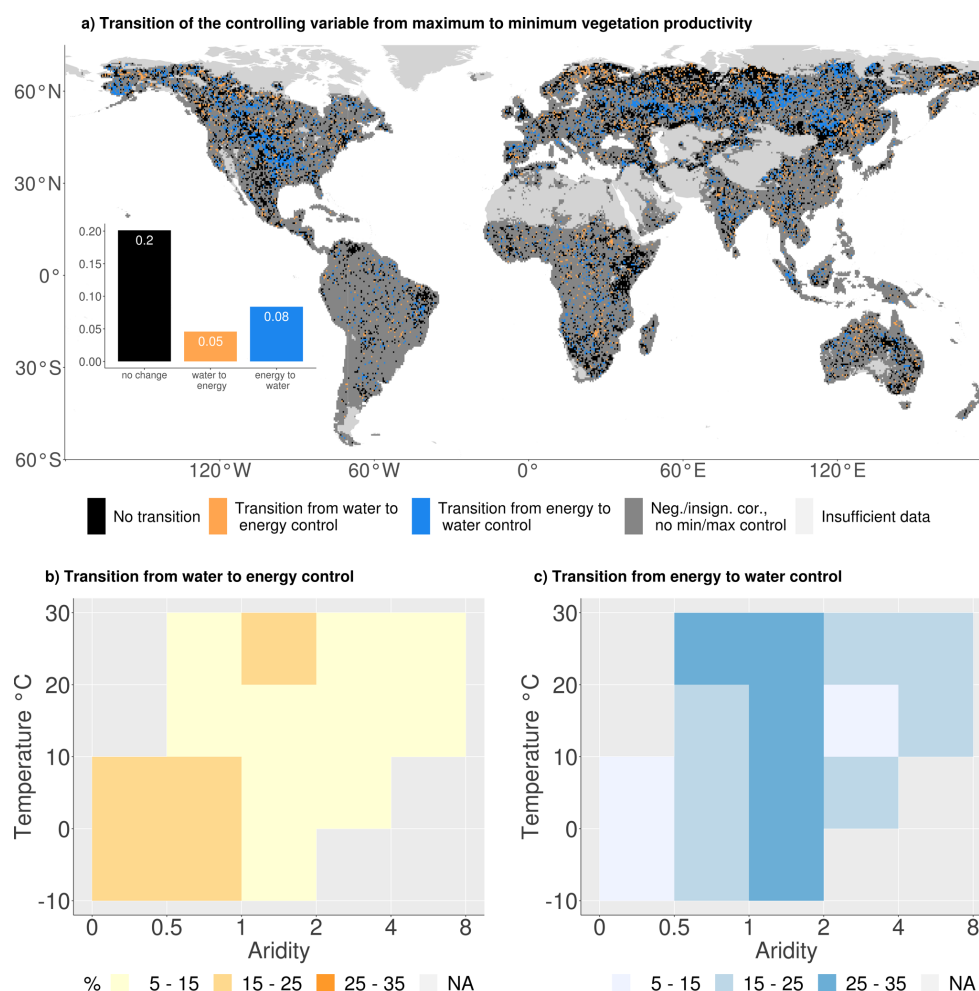


Figure 6. Changing hydrometeorological controls between vegetation productivity maxima and minima. (a) Global distribution of changing controls: In Fig. (b) and (c) grid cells are binned by their long-term climate characteristics. (b) indicates the percentage of grid cells in each climate regime switching from water to energy control, (c) denotes the percentage of grid cells changing from an energy-controlled maxima to a water-controlled minima.

3.6 LIMITATIONS

Our results are obtained at, and valid for, relatively large spatial (half degree) and temporal (monthly) scales. Previous studies have shown differences in the vegetation-climate coupling across scales (Linscheid et al., 2020), suggesting it would be worthwhile to repeat our analysis for different spatiotemporal scales in the future, possibly with new satellite data products. In this context it should be noted, however, that while the relationship between SIF and gross primary productivity (GPP) as actual vegetation productivity is strong for large spatio-temporal scales (Frankenberg et al., 2011; Joiner et al., 2013), it can deteriorate towards smaller scales (He et al., 2020; Maguire et al., 2020; Marrs et al., 2020). And the spatiotemporal range within which there is an acceptable SIF-GPP relationship is not entirely clear yet.

As a second source of uncertainty, SIF data with their relatively large spatial footprint are more vulnerable to cloud contamination compared to finer-scale satellite products (Joiner et al., 2013). Also, especially across South America the SIF data quality is decreased to additional noise (Joiner et al., 2013; Köhler et al., 2015). In our study, many grid cells in these regions and other tropical, cloud-dominated



regions exhibit insignificant or negative correlations between SIF and hydrometeorological anomalies, which is why no hydrometeorological controls can be determined there (Fig. 4). Confirming the validity of our results for the tropical grid cells where results can be obtained, we find mostly consistent and physically meaningful results, e. g. radiation being a main driver of vegetation productivity as the cloud cover is limiting radiation (reported similarly for non-extreme conditions by Green et al., 2020 and Li et al., 2021a).

Next to the SIF data, there is also noteworthy uncertainty in the soil moisture data from ERA5. While data quality of surface soil moisture benefits from (satellite) data assimilation, the soil moisture dynamics in deeper layers are more model-based which is somewhat contradicting the observational character of our study. Therefore, we use soil moisture data from SoMo.ml as an independent data set, which is not based on physical modelling and the related assumptions and parameterizations as it is derived with machine learning applied to in situ measurements from different depths. Overall, the similar results obtained with ERA5-Land and SoMo.ml soil moisture confirm the robustness of our results despite uncertainties in the soil moisture data.

Finally, the use of correlation methods for inferring causal relations is potentially insufficient and under debate (Krich et al., 2020). We want to emphasize that in our study when referring to “drivers” or “controls” of vegetation productivity, we simply base this on correlation and do not imply causality. Nevertheless, we try to filter out confounding effects by disregarding negative and insignificant correlations. Additionally, testing our methodology (approach 2) for non-anomalous vegetation productivity (Fig. S6) which allows to compare results with that of Li et al. (2021a), reveals similar results while they use a different methodology based on random forests and Shapley Additive Explanations (SHAP) values which is more robust against confounding effects. Next to this, in our study we apply two different methodologies in approaches 1 and 2 and find similar results, which further underlines the robustness of our conclusions.

4 CONCLUSION

In this observation-based study, we quantify that vegetation productivity extremes are related to hydrometeorological hazards in about 50% of the global land area that is sufficiently vegetated and cloud-free. The most relevant hazards for vegetation productivity extremes vary along climate gradients. For vegetation productivity maxima the most relevant hydrometeorological extremes are heatwaves in Northern latitudes above 50°N and wet spells in latitudes below 50°N. For productivity minima, drought and cold spells are globally most detrimental to large-scale photosynthesis and carbon uptake. The results of our impact-centric analysis are similar to, and complement more traditional climate-centric studies (Ciais et al., 2005; Flach et al., 2018; Qui et al., 2020). Compound extremes also play a role in 15-20% of our study area, they are somewhat more relevant for productivity minima than for the maxima, with joint drought-heat extremes being most important. Semi-arid, grass-dominated ecosystems tend to transition between water and energy control within the range of their productivity variability. This results in a sensitivity to both water- and energy-related hazards. Thereby, we illustrate how global land-atmosphere coupling hot spots (Koster et al., 2004), where the land surface affects near-surface weather, can be verified using novel vegetation productivity data.

Overall, this study highlights the profound role of (compound) hydrometeorological hazards for global vegetation productivity extremes. Understanding these complex, climate-dependent relationships with present-day observational data is a starting point to more reliably foresee respective changes in a changing future climate with e. g. less cold spells but probably more droughts.

ACKNOWLEDGEMENTS

The authors thank Ulrich Weber for help with obtaining and processing the data. W. Li acknowledges funding from a PhD scholarship from the China Scholarship Council. J.M.C. Denissen, J. Kroll, and R. Orth acknowledge funding by the German Research Foundation (Emmy Noether grant number 391059971).



REFERENCES

- Beer, C., Reichstein, M., Tomelleri, E., Ciais, P., Jung, M., Carvalhais, N., ... & Papale, D.: Terrestrial gross carbon dioxide uptake: global distribution and covariation with climate, *Science*, 329(5993), 834-838, <https://doi.org/10.1126/science.1184984>, 2010.
- Budyko, M. I.: *Climate and life*. Academic press, 1974.
- Ciais, P., Reichstein, M., Viovy, N., Granier, A., Ogée, J., Allard, V., ... & Valentini, R.: Europe-wide reduction in primary productivity caused by the heat and drought in 2003, *Nature*, 437(7058), 529-533, <https://doi.org/10.1038/nature03972>, 2005.
- Denissen, J. M., Teuling, A. J., Reichstein, M., & Orth, R.: Critical soil moisture derived from satellite observations over Europe, *J. Geophys. Res.-Atmos.*, 125(6), <https://doi.org/10.1029/2019JD031672>, 2020.
- Didan, K.: MOD13C1 MODIS/terra vegetation indices 16-day L3 global 0.05 Deg CMG V006, <https://doi.org/10.5067/MODIS/MOD13C1.006>, 2015.
- Fischer, E. M., & Schär, C.: Future changes in daily summer temperature variability: driving processes and role for temperature extremes, *Clim. Dynam.*, 33(7-8), 917, <https://doi.org/10.1007/s00382-008-0473-8>, 2009.
- Flach, M., Sippel, S., Gans, F., Bastos, A., Brenning, A., Reichstein, M., & Mahecha, M. D. (2018). Contrasting biosphere responses to hydrometeorological extremes: revisiting the 2010 western Russian heatwave. *Biogeosciences*, 15(20), <https://doi.org/10.5194/bg-15-6067-2018>, 6067-6085.
- Frankenberg, C., Fisher, J. B., Worden, J., Badgley, G., Saatchi, S. S., Lee, J. E., ... & Yokota, T. (2011). New global observations of the terrestrial carbon cycle from GOSAT: Patterns of plant fluorescence with gross primary productivity. *Geophysical Research Letters*, 38(17), <https://doi.org/10.1029/2011GL048738>.
- Freedman, J. M., Fitzjarrald, D. R., Moore, K. E., & Sakai, R. K.: Boundary layer clouds and vegetation-atmosphere feedbacks, *J. Climate*, 14(2), 180-197, [https://doi.org/10.1175/1520-0442\(2001\)013%3C0180:BLCAVA%3E2.0.CO;2](https://doi.org/10.1175/1520-0442(2001)013%3C0180:BLCAVA%3E2.0.CO;2), 2001.
- Green, J. K., Berry, J., Ciais, P., Zhang, Y., & Gentine, P.: Amazon rainforest photosynthesis increases in response to atmospheric dryness, *Science advances*, 6(47), <https://doi.org/10.1126/sciadv.abb7232>, 2020.
- Guo, Z., & Dirmeyer, P. A.: Interannual variability of land-atmosphere coupling strength, *J. Hydrometeorol.*, 14(5), 1636-1646, <https://doi.org/10.1175/JHM-D-12-0171.1>, 2013.
- Hansen, M., & Song, X. P.: Vegetation continuous fields (VCF) yearly global 0.05 deg. NASA EOSDIS Land Processes DAAC, 645, <https://doi.org/10.5067/MEaSURES/VCF/VCF5KYR.001>, 2018.
- He, L., Magney, T., Dutta, D., Yin, Y., Köhler, P., Grossmann, K., ... & Frankenberg, C.: From the ground to space: Using solar-induced chlorophyll fluorescence to estimate crop productivity, *Geophys. Res. Lett.*, 47(7), <https://doi.org/10.1029/2020GL087474>, 2020.
- Hersbach, H., Bell, B., Berrisford, P., Hirahara, S., Horányi, A., Muñoz-Sabater, J., ... & Thépaut, J. N.: The ERA5 global reanalysis, *Q. J. Roy. Meteor. Soc.*, 146(730), 1999-2049, <https://doi.org/10.1002/qj.3803>, 2020.
- Hong, X., Leach, M. J., & Raman, S.: A sensitivity study of convective cloud formation by vegetation forcing with different atmospheric conditions, *J. Appl. Meteorol. Clim.*, 34(9), 2008-2028, [https://doi.org/10.1175/1520-0450\(1995\)034%3C2008:ASSOCC%3E2.0.CO;2](https://doi.org/10.1175/1520-0450(1995)034%3C2008:ASSOCC%3E2.0.CO;2), 1995.
- Joiner, J., Yoshida, Y., Vasilkov, A. P., Yoshida, Y., Corp, L. A., and Middleton, E. M.: First observations of global and seasonal terrestrial chlorophyll fluorescence from space, *Biogeosciences*, 8, 637-651, <https://doi.org/10.5194/bg-8-637-2011>, 2011.



- 415
 416 Joiner, J., Guanter, L., Lindstrot, R., Voigt, M., Vasilkov, A. P., Middleton, E. M., Huemmrich, K. F., Yoshida, Y., and
 417 Frankenberg, C.: Global monitoring of terrestrial chlorophyll fluorescence from moderate-spectral-resolution
 418 near-infrared satellite measurements: methodology, simulations, and application to GOME-2, *Atmos. Meas.*
 419 *Tech.*, 6, 2803–2823, <https://doi.org/10.5194/amt-6-2803-2013>, 2013.
 420 Koster, R. D., Dirmeyer, P. A., Guo, Z., Bonan, G., Chan, E., Cox, P., ... & Yamada, T.: Regions of strong coupling
 421 between soil moisture and precipitation, *Science*, 305(5687), 1138–1140,
 422 <https://doi.org/10.1126/science.1100217>, 2004.
 423
 424 Köhler, P., Guanter, L., and Joiner, J.: A linear method for the retrieval of sun-induced chlorophyll fluorescence
 425 from GOME-2 and SCIAMACHY data, *Atmos. Meas. Tech.*, 8, 2589–2608, [https://doi.org/10.5194/amt-8-2589-](https://doi.org/10.5194/amt-8-2589-2015)
 426 [2015](https://doi.org/10.5194/amt-8-2589-2015), 2015.
 427
 428 Krich, C., Runge, J., Miralles, D. G., Migliavacca, M., Perez-Priego, O., El-Madany, T., Carrara, A., and Mahecha, M.
 429 D.: Estimating causal networks in biosphere–atmosphere interaction with the PCMCi approach, *Biogeosciences*,
 430 17, 1033–1061, <https://doi.org/10.5194/bg-17-1033-2020>, 2020.
 431
 432 Li, W., Migliavacca, M., Forkel, M., Walther, S., Reichstein, M., & Orth, R.: Revisiting Global Vegetation Controls
 433 Using Multi-Layer Soil Moisture, *Geophys. Res. Lett.*, 48(11), <https://doi.org/10.1029/2021GL092856>, 2021a.
 434
 435 Li, J., Tam, C. Y., Tai, A. P., & Lau, N. C.: Vegetation-heatwave correlations and contrasting energy exchange
 436 responses of different vegetation types to summer heatwaves in the Northern Hemisphere during the 1982–
 437 2011 period, *Agr. Forest Meteorol.*, 296, <https://doi.org/10.1016/j.agrformet.2020.108208>, 2021b.
 438
 439 Li, X., & Xiao, J.: Global climatic controls on interannual variability of ecosystem productivity: Similarities and
 440 inferences inferred from solar-induced chlorophyll fluorescence and enhanced vegetation index, *Agr. Forest*
 441 *Meteorol.*, 288, <https://doi.org/10.1016/j.agrformet.2020.108018>, 2020.
 442
 443 Linscheid, N., Estupinan-Suarez, L. M., Brenning, A., Carvalhais, N., Cremer, F., Gans, F., Rammig, A., Reichstein,
 444 M., Sierra, C. A., and Mahecha, M. D.: Towards a global understanding of vegetation–climate dynamics at
 445 multiple timescales, *Biogeosciences*, 17, 945–962, <https://doi.org/10.5194/bg-17-945-2020>, 2020.
 446
 447 Madani, N., Kimball, J. S., Jones, L. A., Parazoo, N. C., & Guan, K.: Global analysis of bioclimatic controls on
 448 ecosystem productivity using satellite observations of solar-induced chlorophyll fluorescence, *Remote Sens-*
 449 *Basel* 9(6), 530, <https://doi.org/10.3390/rs9060530>, 2017.
 450
 451 Magney, T. S., Barnes, M. L., & Yang, X.: On the covariation of chlorophyll fluorescence and photosynthesis
 452 across scales, *Geophys. Res. Lett.*, 47(23), <https://doi.org/10.1029/2020GL091098>, 2020.
 453
 454 Maguire, A. J., Eitel, J. U., Griffin, K. L., Magney, T. S., Long, R. A., Vierling, L. A., ... & Bruner, S. G.: On the
 455 functional relationship between fluorescence and photochemical yields in complex evergreen needleleaf
 456 canopies, *Geophys. Res. Lett.*, 47(9), <https://doi.org/10.1029/2020GL087858>, 2020.
 457
 458 Marrs, J. K., Reblin, J. S., Logan, B. A., Allen, D. W., Reinmann, A. B., Bombard, D. M., ... & Hutrya, L. R.: Solar-
 459 induced fluorescence does not track photosynthetic carbon assimilation following induced stomatal closure,
 460 *Geophys. Res. Lett.*, 47(15), <https://doi.org/10.1029/2020GL087956>, 2020.
 461
 462 Muñoz Sabater, J.: ERA5-Land monthly averaged data from 1981 to present, Copernicus Climate Change Service
 463 (C3S) Climate Data Store (CDS), <https://doi.org/10.24381/cds.68d2bb30>, 2019.
 464
 465 O, S., Dutra, E., & Orth, R.: Robustness of process-based versus data-driven modeling in changing climatic
 466 conditions, *J. Hydrometeorol.*, 21(9), 1929–1944, <https://doi.org/10.1175/JHM-D-20-0072.1>, 2020.
 467
 468 O, S. & Orth, R.: Global soil moisture data derived through machine learning trained with in-situ measurements,
 469 *Scientific Data*, 8(1), 1–14, <https://doi.org/10.1038/s41597-021-00964-1>, 2021.
 470



- Orth, R., Destouni, G., Jung, M., and Reichstein, M.: Large-scale biospheric drought response intensifies linearly with drought duration in arid regions, *Biogeosciences*, 17, 2647–2656, <https://doi.org/10.5194/bg-17-2647-2020>, 2020.
- Orth, R.: When the land surface shifts gears. *AGU Advances*, 2(2), <http://dx.doi.org/10.1029/2021AV000414>, 2021.
- Otu-Larbi, F., Bolas, C. G., Ferracci, V., Staniaszek, Z., Jones, R. L., Malhi, Y., ... & Ashworth, K.: Modelling the effect of the 2018 summer heatwave and drought on isoprene emissions in a UK woodland, *Glob. Change Biol.*, 26(4), 2320–2335, <https://doi.org/10.1111/gcb.14963>, 2020.
- Piao, S., Wang, X., Wang, K., Li, X., Bastos, A., Canadell, J. G., ... & Sitch, S.: Interannual variation of terrestrial carbon cycle: Issues and perspectives, *Glob. Change Biol.*, 26(1), 300–318, <https://doi.org/10.1111/gcb.14884>, 2020.
- Pielke Sr, R. A., Adegoke, J., Beltraán-Przekurat, A., Hiemstra, C. A., Lin, J., Nair, U. S., ... & Nobis, T. E.: An overview of regional land-use and land-cover impacts on rainfall, *Tellus B*, 59(3), 587–601, <https://doi.org/10.1111/j.1600-0889.2007.00251.x>, 2007.
- Prein, A. F., & Heymsfield, A. J.: Increased melting level height impacts surface precipitation phase and intensity, *Nat. Clim. Change*, 10(8), 771–776, <https://doi.org/10.1038/s41558-020-0825-x>, 2020.
- Qiu, B., Ge, J., Guo, W., Pitman, A. J., & Mu, M.: Responses of Australian dryland vegetation to the 2019 heat wave at a subdaily scale, *Geophys. Res. Lett.*, 47(4), <https://doi.org/10.1029/2019GL086569>, 2020.
- Seddon, A. W., Macias-Fauria, M., Long, P. R., Benz, D., & Willis, K. J.: Sensitivity of global terrestrial ecosystems to climate variability, *Nature*, 531(7593), 229–232, <https://doi.org/10.1038/nature16986>, 2016.
- Turner, D. P., Cohen, W. B., Kennedy, R. E., Fassnacht, K. S., & Briggs, J. M.: Relationships between leaf area index and Landsat TM spectral vegetation indices across three temperate zone sites, *Remote Sens. Environ.*, 70(1), 52–68, [https://doi.org/10.1016/S0034-4257\(99\)00057-7](https://doi.org/10.1016/S0034-4257(99)00057-7), 1999.
- Turner, A. J., Köhler, P., Magney, T. S., Frankenberg, C., Fung, I., and Cohen, R. C.: A double peak in the seasonality of California's photosynthesis as observed from space, *Biogeosciences*, 17, 405–422, <https://doi.org/10.5194/bg-17-405-2020>, 2020.
- Walther, S., Voigt, M., Thum, T., Gonsamo, A., Zhang, Y., Köhler, P., ... & Guanter, L.: Satellite chlorophyll fluorescence measurements reveal large-scale decoupling of photosynthesis and greenness dynamics in boreal evergreen forests, *Glob. Change Biol.*, 22(9), 2979–2996, <https://doi.org/10.1111/gcb.13200>, 2016.
- Wang, X., Qiu, B., Li, W., & Zhang, Q.: Impacts of drought and heatwave on the terrestrial ecosystem in China as revealed by satellite solar-induced chlorophyll fluorescence, *Sci. Total Environ.*, 693, <https://doi.org/10.1016/j.scitotenv.2019.133627>, 2019.
- Zscheischler, J., Mahecha, M. D., Harmeling, S., & Reichstein, M.: Detection and attribution of large spatiotemporal extreme events in Earth observation data, *Ecol. Inform.*, 15, 66–73, <https://doi.org/10.1016/j.ecoinf.2013.03.004>, 2013.
- Zscheischler, J., Mahecha, M. D., Von Buttlar, J., Harmeling, S., Jung, M., Rammig, A., ... & Reichstein, M.: A few extreme events dominate global interannual variability in gross primary production, *Environ. Res. Lett.*, 9(3), <https://doi.org/10.1088/1748-9326/9/3/035001>, 2014a.
- Zscheischler, J., Reichstein, M., Harmeling, S., Rammig, A., Tomelleri, E., and Mahecha, M. D.: Extreme events in gross primary production: a characterization across continents, *Biogeosciences*, 11, 2909–2924, <https://doi.org/10.5194/bg-11-2909-2014>, 2014b.
- Zhang, L., Qiao, N., Huang, C., & Wang, S.: Monitoring drought effects on vegetation productivity using satellite solar-induced chlorophyll fluorescence, *Remote Sens.-Basel*, 11(4), 378, <https://doi.org/10.3390/rs11040378>, 2019.



529
530 Zhao, M., & Running, S. W.: Drought-induced reduction in global terrestrial net primary production from 2000
531 through 2009, *Science*, 329(5994), 940-943, <https://doi.org/10.1126/science.1192666>, 2010

532